

EIGHTH EUROPEAN ROTORCRAFT FORUM

Paper No 2.9

AN ANALYTICAL THEORY FOR ROTOR-
TIPVANE PERFORMANCE AND COMPARISON
WITH EXPERIMENTAL RESULTS

Th. VAN HOLTEN

DELFT UNIVERSITY OF TECHNOLOGY
DEPARTMENT OF AEROSPACE ENGINEERING

August 31 through September 3, 1982

AIX-EN-PROVENCE, FRANCE

ASSOCIATION AERONAUTIQUE ET ASTRONAUTIQUE DE FRANCE

AN ANALYTICAL THEORY FOR ROTOR-
TIPVANE PERFORMANCE AND COMPARISON
WITH EXPERIMENTAL RESULTS

Th. van Holten

DELFT UNIVERSITY OF TECHNOLOGY
DEPARTMENT OF AEROSPACE ENGINEERING

Summary

A theoretical method for the performance estimation of tipvane wind turbines is outlined in the paper, and compared with some full-scale experimental results recently obtained. The performance estimates are based on a flowmodel where an infinite number of turbine blades is assumed. Agreement between theory and experiments is shown to be satisfactory.

1. Introduction

At the Delft University of Technology research is done on tipvane windturbines. Tipvanes are relatively small auxiliary wings mounted on the tips of turbine-blades (fig. 1). The vane lift is in the direction of the rotorcentre so that by reaction the oncoming flow is deflected radially outwards. The resulting diffuser effect causes an increase of massflow through the turbine (fig. 2). Compared with conventional turbines, higher powercoefficients are possible, even surpassing the so-called Betz-limit for windturbines.

The laboratory research has covered windtunnel- and towing tank model experiments (ref. 1). Full-scale performance testing has started recently on a 8,5 m diameter rotor. In view of the lack of experience with rotors of such an unconventional configuration, careful theoretical and experimental aero-elastic investigations on the full-scale rotor have preceded the aerodynamic experiments (ref. 2 and 3). The aerodynamic investigations were likewise accompanied by the development of theory:

- a) computer programs were developed for the detailed analysis of load-distributions (ref. 4),
- b) a flowmodel based on the assumption of an infinite number of blades was developed for the purpose of performance estimates.

It is the latter analysis which will be briefly outlined in the present paper, and the results of which will be compared with some preliminary full-scale test-results now available.

2. Analytical model of the flow

The model described below was developed with the purpose to analyze the overall forces, total power, and average velocities. It assumes an infinite number of turbineblades and tipvanes. Such a model of the flow is equivalent to a time-averaged analysis. The model is based on the assumption of small disturbances, which means that free vorticity convects along trajectories parallel to the undisturbed velocity.

2.1 Tipvane-model

The functioning of the tipvanes is represented by a circular band of vorticity as sketched in fig. 3. The way to arrive at such a simplified flow model will be explained with the help of fig. 4, which shows so-called "undersynchronous operation", i.e. a flowcondition where no direct vortex interaction occurs. We assume for a moment that the lift on the tipvanes is constant along the span, so that the trailing vorticity is concentrated in two discrete tipvortices. In linearized theory these vortices lie on a straight cylindrical surface with radius R and trace out helical paths. The flow associated with this vortex configuration is unsteady in an inertial frame of reference. The time averaged flow

field is obtained by taking the limit of an infinite number of tipvanes, taking care that the same radial force per unit length along the turbine circumference is generated by the infinite array of tipvanes as by the finite number of tipvanes. The helical vortices in this limit form a continuous, semi-infinite vortex-cylinder. Now it should be remembered that the tipvorticity emanating from the upstream vane-tips has equal strength but opposite direction compared with the trailing vorticity from the downstream vane-tips. The two vortex-cylinders associated with the upstream and downstream vane-tips cancel each other, except for a band of vorticity with a width equal to the span of the tipvanes. We have thus arrived at the model of fig. 3. When the vane-lift points towards the centre-line of the turbine, an overall circulation is established with such a direction that the vortex band induces a Venturi-type of flow like in fig. 2. A more careful analysis given in ref. 5 shows that the same is true for the case of general spanwise lift distributions along the tipvanes.

The average velocity increment in the disc plane due to the functioning of the tipvanes will be denoted by $\overline{\delta V}$, and may be expressed like:

$$\overline{\delta V} = \alpha \cdot \frac{\Gamma}{R} \quad (1)$$

where Γ stands for the total circulation of the circumferential band of vorticity. The proportionality constant α is a function of the spanwise lift distribution along the tipvanes. According to an asymptotic analysis given in ref. 6, in the case of an elliptic distribution it is given by:

$$\alpha = \frac{1}{\pi} \left\{ \ln \left(\frac{4}{b_e/R} \right) + \frac{1}{2} \right\} \quad (2)$$

where b_e is the effective span, i.e. the part of the span where due to vortex interactions (explained below) most of the lift is concentrated.

The radial distribution of the velocity $\delta V(x)$, (where $x = r/R$), induced by the vortex band may be approximated by:

$$\delta V(x) \cdot \frac{2\pi R}{\Gamma} = \pi - \left\{ \pi - \delta V(1) \frac{2\pi R}{\Gamma} \right\} e^{-A(1-x)} \quad (3)$$

where

$$\delta V(1) \cdot \frac{2\pi R}{\Gamma} = \frac{4}{b_e/R} \left(1 - \frac{b_e/R}{16} \right) - \frac{1}{2} \ln \left(\frac{b_e/R}{32} \right) \quad (4)$$

$$A = \frac{1}{2C} + \frac{1}{2C} \sqrt{1 - 4C} \quad (5)$$

with

$$C = \frac{\pi/2 - \alpha \cdot \pi}{\pi - \delta V(1) \frac{2\pi R}{\Gamma}} \quad (6)$$

The band of vorticity associated with the tipvanes induces in its own plane an axial velocity δw of an average magnitude

$$\delta w = \beta \cdot \frac{\Gamma}{R} \quad (7)$$

This selfinduction velocity δw corresponds to the convection velocity of a free vortex ring in still air. The proportionality constant β is, again according to the analysis of ref. 6, given by:

$$\beta = \frac{1}{4\pi} \cdot \left\{ \ln \left(\frac{32}{b_e/R} \right) - \frac{5}{6} \right\} \quad (8)$$

The above given theory remains valid in the limiting case of "synchronous" operation, i.e. the flow condition where the vortex from the upstream vane-edge

just touches the downstream edge of the next vane.

We now proceed to the case of so-called "over-synchronous" operation, i.e. a condition where strong vortex-interaction occurs. In fig. 5 the array of tip-vanes is drawn in a flat plane as if one were looking down on a formation flight of birds. Looking from the rear of the formation there is a certain amount of overlap of the wingspans so that a part of each vane is immersed in the downwash of the preceding one. Fig. 6 shows the resulting lift distribution along a vane, as calculated by the methods described in ref. 4. It is seen that the part of the span which is immersed in a downwash region loses its lift. As a consequence the tipvortex originating in this region of the vane is shifted inboard, towards the edge of the more effective part of the vane. This trailing vortex is thus shifted towards the point where the vane is "hit" by the tipvortex of the preceding vane (fig. 5). The result is, that the newly formed tipvortex and the vortex from the preceding vane almost entirely annihilate each other. What has been left is a "saw-tooth" vortex running from vane to vane, roughly forming a vortex ring around the turbine (fig. 7). Numerous flow visualisations have confirmed the actual occurrence of the saw tooth vortex. The saw tooth vortex of the real flow is in fact the same as the vortex band of the linearized flowmodel of fig. 3, be it in a rolled-up form. The model of fig. 3 and the results (1) through (8) are applicable to both under- and over-synchronous operation, since the strong vortex interactions in fact result in synchronous operation at an effectively reduced span b_e (so-called "auto-synchronization"). The total circulation Γ may now be related to the lift of the vane by considering the bound part of the saw-tooth:

$$\Gamma = \frac{1}{2} \hat{C}_\ell c \Omega R \quad (9)$$

where \hat{C}_ℓ is the maximum liftcoefficient occurring somewhere along the vane-span. In the saw tooth model the liftcoefficient would equal \hat{C}_ℓ for all the sections along a part of the span equal to b_v where b_v (the so-called "vortex span") is the lateral distance between the free branches of the saw tooth vortex. In the real flow, C_ℓ varies more smoothly along the vane-span of course (see fig. 6). We may write:

$$\hat{C}_\ell = C_L \cdot \frac{b}{b_v} \quad (10)$$

and by combining eqs. (9) and (1) it is thus found:

$$\frac{\overline{\delta V}}{U} = \frac{\alpha}{2} \cdot C_L \frac{c}{R} \frac{b}{b_v} \cdot \lambda \quad (11)$$

where $\lambda = \text{tipspeed - ratio } \Omega R/U$

Finally, in fig. 8 an even more general flow-state has been sketched such as often occurs during "off-design" conditions. The trailing vortex sheet rolls up into a tipvortex at A, which drifts along with the local flow after the passing of the vane. The average convection velocity of the vortex is denoted vectorially by \underline{W} (lower part of fig. 8). In general \underline{W} is not parallel to the free stream velocity \underline{U} due to the functioning of the powerturbine which induces a radial flow component. Upon arrival of the next vane, the vortex has drifted from A to B at which position by the previously explained flowmechanisms it causes the release of a new, counterrotating vortex at C. It is seen that in this case too the eqs (1) to (10) may be used. The "vortex-span ratio" is from fig. 8:

$$\frac{b_v}{b} = \frac{2\pi}{N} \cdot \frac{R}{b} \frac{1}{\lambda} \cdot \frac{W}{U} \quad (12)$$

where $N =$ number of tipvanes.

The tip speed ratio where the vane-span becomes too short to "intercept" the free vortex at B depends, apart from the span, on the "rolling-up offset-distance" kb_e (see fig. 8) which for a rectangular vane planform typically has a value of the order $0,1 \cdot b_e$.

2.2 Turbinemodel

For the functioning of the powerturbine the well-known model of a semi-infinite vortex tube is used. The axial velocity induced by the vortex cylinder in the disc plane is v_i and far downstream $2v_i$ (fig. 3). Velocities in the surface of the vortex-cylinder itself have half this value. Thus, the powerturbine induces exactly at its entrance-lip an axial velocity $\frac{1}{2}v_i$ which must be taken into account when the local flow environment experienced by the tipvanes is analyzed.

2.3 Model for wake mixing

Turbulent mixing of the wake flow with the surrounding flow is for propeller- or windturbineperformance usually considered unimportant. In contrast, in the case of a tipvane turbine wake mixing effects are found to have an important influence. The Venturi-type of flow through a tipvane-turbine leads to a much larger wake expansion and consequently also to a much longer and wider wake region with sub-ambient pressures compared with the conventional turbine.

Since the wake flow is not shielded from the external flow by a material wall, some amount of mixing always occurs in this region of reduced pressure.

The resulting situation is shown schematically in fig. 9 which should be compared with fig. 2.

In the flows without mixing (fig. 2), a certain minimum value of the final wake velocity is needed in order to ensure a positive mass flow through the system and to prevent the flow from collapsing into the turbulent wake state. In fig. 9, however, the turbine can extract more energy per unit of mass flow before encountering the turbulent wake state, since the minimum value of the velocity now occurs at the "entrance" of the "low pressure reservoir". At this point not only kinetic energy has been given up by the fluid, but also some potential energy. Due to mixing in the low pressure reservoir with a stream of secondary air, there is momentum added to the turbine flow before it is finally exhausted into the ambient atmosphere. The effect is usually called "ejector effect", since there is some resemblance with an ejector pump placed behind the turbine. The effect of wake mixing may, alternatively, be compared with the effect of a favourable pressure gradient in the ambient air. A favourable gradient would in the same way postpone the occurrence of the turbulent wake state by relaxing the condition that the final wake pressure must come back to the undisturbed pressure.

The turbulent mixing process itself can at present not yet be brought into a simple analytical model. The ultimate effect of the turbulent mixing can be modelled simply, by introducing an element into the analytical model which simulates a reduced "back pressure" experienced by the turbine. The additional analytical element must preferably be a solution of the potential equation so that one is certain that the fundamental conservation laws of the flow are not violated. The simplest simulation of the ejector-effect by an element consistent with potential theory is a vortex ring having large dimensions compared with the wake, and placed sufficiently far downstream so that it does not induce in any direct way additional velocities in the turbine plane.

Denoting the additional velocity induced by the vortex ring at "infinity" by δv_e , application of Bernoulli's theory to the flow outside the wake yields the pressure p_e in the far wake:

$$\frac{p_e - p_o}{\frac{1}{2} \rho U^2} = - \frac{\overline{\delta v_e}}{U} \left(2 + \frac{\overline{\delta v_e}}{U} \right) \quad (13)$$

3. Momentum-analysis of the tipvane turbine

A control-volume will be considered as shown in fig. 3. Within this volume three kinds of external forces may be discerned:

- a. An axial force D_{ax} exerted on the air by the power turbine. It is written in non-dimensional form as

$$C_{D_{ax_1}} = \frac{D_{ax}}{\frac{1}{2}\rho U^2 \pi R^2} \quad (14)$$

- b. An axial force of the magnitude $N.L_{\text{vanes}} \sin(\gamma_{id})$. As was shown in fig. 8 the span of the vanes must be inclined somewhat, so that the freely convecting vane-vortices are exactly intercepted by the next vane. When the local flow-direction is γ_{id} (= ideal tiltangle of the vane-span) the vane lift gives rise to the above given axial force, or in non-dimensional form: $C_{D_{ax_2}} =$

$$C_L \cdot \sigma_v \cdot \lambda^2 \cdot \gamma_{id} \quad \text{where } \sigma_v = \frac{N.S_{\text{vane}}}{\pi R^2} \text{ is the vane-solidity.}$$

- c. It is also shown in fig. 8 that for an arbitrary tiltangle $\gamma \neq \gamma_{id}$ the vane-vortex system is not exactly closed, and will locally accelerate or decelerate a part of the fluid. The non-dimensional force associated with this addition to the turbine-function is $C_{D_{ax_3}} = C_L \sigma_v \cdot \lambda^2 (\gamma - \gamma_{id})$.

The volume of air Q entering the control-volume through the sides is per unit time:

$$Q = A \cdot \overline{\delta v}_e - 2v_i \pi r_e^2 \quad (15)$$

with A = frontal area of the control surface, and r_e = radius of final wake. It is found that this volume of air must be assumed to have an average axial velocity $U + \frac{1}{2} \cdot \overline{\delta v}_e$, in order to make the final results independent from A , as they should be. The momentum conservation law applied to the whole of the control volume then yields:

$$C_{D_{ax_1}} + C_{D_{ax_2}} + C_{D_{ax_3}} = 4 \cdot \frac{\overline{v}_i}{U} \left(1 - \frac{\overline{v}_i}{U} + \frac{\overline{\delta v}_e}{U}\right) + 2 \cdot \frac{\overline{v}_i}{U} \frac{\overline{\delta v}_e}{U} \cdot \frac{1 - \frac{\overline{v}_i}{U} + \frac{\overline{\delta v}_e}{U}}{1 - 2 \frac{\overline{v}_i}{U} + \frac{\overline{\delta v}_e}{U}} \quad (16)$$

Both the forces $C_{D_{ax_1}}$ and $C_{D_{ax_3}}$ change the total pressure of the flow, in contrast to the force $C_{D_{ax_2}}$. Application of Bernoulli's law along a streamline from

far upstream to a point immediately upstream of the discplane, as well as applying it along a streamline running from immediately downstream of the discplane to far downstream, yields:

$$C_{D_{ax_1}} + C_{D_{ax_3}} = 4 \cdot \frac{\overline{v}_i}{U} \left(1 - \frac{\overline{v}_i}{U} + \frac{\overline{\delta v}_e}{U}\right) \quad (17)$$

Subtracting (17) from (16):

$$C_{D_{ax_2}} = 4 \cdot \frac{\bar{v}_i}{U} \left(\frac{\delta \bar{v}}{U} - \frac{\delta \bar{v}_e}{U} \right) +$$

$$+ 2 \cdot \frac{\bar{v}_i}{U} \cdot \frac{\delta \bar{v}_e}{U} \cdot \frac{1 - \frac{\bar{v}_i}{U} + \frac{\delta \bar{v}}{U}}{1 - 2 \frac{\bar{v}_i}{U} + \frac{\delta \bar{v}_e}{U}} \quad (18)$$

The quantities \bar{v}_i and $\delta \bar{v}_e$ occurring in (17) denote average velocities. We can by analogy with the usual propeller-analysis, also apply (17) to individual annuli of the flow. When doing so, it should be remembered that the term $C_{D_{ax_3}}$ indicates the axial force in an outer shell of the wake surrounding the wake of the power turbine itself. The induced velocity in the inner annuli is thus found from the expression:

$$\frac{v_i}{U}(x) = \frac{1}{2} \{1 + \delta v_e/U(x)\} - \frac{1}{2} \cdot \sqrt{\{1 + \delta v_e/U(x)\}^2 - C_{d_{ax}}(x)} \quad (19)$$

It should be emphasized, that eq. (19) would not follow from a straightforward application of momentum theory to the individual flow annuli, the reason being that the pressure forces on the annuli-surfaces do not cancel out. The axial force $C_{D_{ax_2}}$ due to the tipvanes is "transmitted" via such pressure forces to the individual annuli with the result that the correct momentum balance is restored per annulus.

According to the velocity diagram of fig. 10:

$$C_{d_{ax}}(x) = C_l(x) \cdot \sigma(x) \cdot \lambda^2 x^2 =$$

$$= \left\{ \frac{1 - \frac{v_i}{U}(x) + \frac{\delta v}{U}(x)}{\lambda x} - \theta(x) \right\} \cdot \sigma(x) \lambda^2 x^2 \quad (20)$$

with $x = r/R$ and $\sigma = \frac{Nc}{2\pi r}$.

It is seen from (19) that the value of $C_{d_{ax}}$ where the flow in the annulus breaks down into a turbulent wake state is given by

$$(C_{d_{ax}})_{\max} = \{1 + \delta v_e/U(x)\}^2 \quad (21)$$

By means of (21) the strength of the ejector-effect may be estimated empirically from experiments.

When the value of the vane lift coefficient C_L is known the system of equations so far derived is sufficient to determine quantitatively the performance of the power turbine in the presence of tipvanes.

The performance of the vanes themselves (C_L and C_D) cannot be predicted by the theory derived above. The momentum considerations do, however, provide us with the flow-angles experienced by the tipvanes, since γ_{id} is known from (18) and the local velocity w of fig. 8 is given by

$$w = U \cdot \left\{ 1 - \frac{1}{2} \frac{\bar{v}_i}{U} + \frac{\beta}{\alpha} \cdot \frac{\delta \bar{v}}{U} \right\} \quad (22)$$

4. Tipvane performance

Simple geometry gives the mean angle of attack α of the effective part of the vane:

$$\alpha = \theta - \sin\gamma \sin\Lambda - \frac{W}{U} \cdot \frac{1}{\lambda} (\gamma - \gamma_{id}) - \frac{v_{i \text{ vane}}}{\Omega R} \quad (23)$$

The first term θ is the geometrical incidence of the vanes (nose-in positive, so that the positive lift direction is towards the rotor centre). The second term is associated with the rotational velocity ΩR , which has a component perpendicular to the vane-surface when both the tilt angle γ and the yaw-angle Λ are non-zero.

The third term gives the effect of a non-ideal tilt-angle, i.e. such a tilt-angle that the span is not parallel to the local velocity \underline{W} . Finally the fourth term represents, what in classical wing theory is called the induced angle of attack. For a brief outline of the determination of the induced angle of attack we again consider the array of tipvanes as a formation of wings. The Trefftz plane is drawn in fig. 11. W . r. to the first wing an elliptical coordinate system (η, φ) is fixed, defined by:

$$\begin{aligned} x &= \frac{1}{2} b_e \cosh \eta \cdot \cos \varphi \\ y &= \frac{1}{2} b_e \sinh \eta \cdot \sin \varphi \end{aligned} \quad (24)$$

The two-dimensional velocity potential in the Trefftz plane due to an elliptical lift distribution along the effective span b_e is given by:

$$\phi = b_e \cdot \Omega R \cdot \frac{C_{L_e}}{\pi A_e} e^{-\eta} \sin \varphi \quad (25)$$

where the quantities C_{L_e} and the aspect ratio A_e are both referred to the effective span b_e (see L_e for the value of b_e fig. 8). The induced velocity caused by the entire formation of wings and wakes is then found to be:

$$v_{i \text{ vane}} = \Omega R \cdot \frac{C_{L_e}}{\pi A_e} (1 - \cos \varphi_0 \cdot e^{-\eta_0}) \quad (26)$$

where the point (η_0, φ_0) indicates the position of the edge of the first "returning" vortex sheet closest to the vane under consideration (point B in fig. 8).

It is seen that in the case of perfect vortex-synchronization (i.e. when B and C in fig. 8 coincide) there is no induced velocity $v_{i \text{ vane}}$ since $\varphi_0 = 0$ and $\eta_0 = 0$. On the other hand, when there is a large gap between B and C ($\eta_0 \rightarrow \infty$), the classical result of a single wing is obtained. Since the position of B is to a certain extent determined by the roll-up offset distance kb_e , a small overlap of the geometrical projections of the wings on the Trefftz plane is needed before perfect vortex-synchronization occurs.

Now multiplying eq. (23) by the two-dimensional lift-curve slope C_{l_α} and substituting (26) into it, we find:

$$C_{L_e} = \frac{C_{l_\alpha}}{1 + \frac{C_{l_\alpha}}{\pi A_e} (1 - \cos \varphi_0 \cdot e^{-\eta_0})} \cdot \left\{ \theta - \sin\gamma \sin\Lambda - \frac{W}{U} \frac{1}{\lambda} (\gamma - \gamma_{id}) \right\} \quad (27)$$

whereas the vane-dragcoefficient is by a similar analysis found to be:

$$C_{D_i} = \frac{C_{L_e}^2}{\pi A_e} (1 - \cos \varphi_o e^{-\eta_o}) - C_{L_e} \cdot \frac{W}{U} \cdot \frac{1}{\lambda} (\gamma - \gamma_{id}) \quad (28)$$

The latter result shows that in the case of perfect vortex-synchronization the induced drag coefficient of a tipvane is zero.

5. Experimental verification

For the purpose of verification of the outlined theory, numerous experiments have been done in windtunnels and in a towing-tank, whereas also full-scale tests on a 8,5 meter diameter tipvane rotor have recently started and have already yielded some preliminary results.

Ref. 1 describes in slightly more detail the windtunnel and towing-tank experiments. A few results will be given below.

Fig. 12 shows measured and calculated characteristics of a windtunnelmodel in which the turbine was simulated by gauzes around which tipvanes were rotating. Pitot-static tube traverses behind the gauzes were made to determine velocities and total pressures. In the diffuser diagram of fig. 12 these are shown in integrated form, with turbine blockage C_D on the horizontal axis and the total velocity through the simulated turbine ax_1 along the vertical axis. The large centrifugal forces acting on the tipvanes prevented liftmeasurements to be made on the tipvanes, so that the latter measurements had to be done on a geometrically similar model in a towing tank. Although the experiments in water were only partially succesfull, the general level of vane liftcoefficients predicted by the theory was confirmed.

Fig. 13 shows a typical distribution of velocity and total pressure, measured and calculated for the same test set-up as above.

Fig. 14 shows measurements of tipvane-drag. As indicated by equation (28), correct vortex synchronization will lead to a flowstate where the tipvanes do not experience induced drag. This is confirmed by fig. 14.

Fig. 1 shows the 8.5 m diameter rotor used for full-scale tests and fig. 15 gives some preliminary results of measured and predicted performance. It should be stressed that the configuration is not yet optimized (the vane lift can be increased further, whereas powerblades will later be mounted having slightly more twist).

6. Conclusions

Relatively simple theory based on the assumption of an infinite number of blades can be derived for tipvane-windturbines. A satisfactory agreement between theory and experiments is found.

7. References

1. Th. van Holten, Concentrator systems for wind energy, with emphasis on tipvanes, Wind Engineering Vol. 5 No. 1, 1981.
2. P.C. Hensing and J.J.W. Opdam, The influence of a tipvane on the aeroelastic stability of a rotorblade. Part I: Mechanical influences, Report LR-274, Delft University of Technology, Department of Aerospace Engineering.
3. G.J.W. van Bussel, P.C. Hensing and G.A.M. van Kuik, Aerodynamic and Aeroelastic Research on Tipvane Turbines, Report LR-302, Delft University of Technology, Department of Aerospace Engineering.
4. G.J.W. van Bussel, Th. van Holten, G.A.M. van Kuik, Aerodynamic Research on Tipvane Windturbines, AGARD Conference Preprint No. 334, Prediction of Aerodynamic Loads on Rotorcraft, April 1982.

5. Th. van Holten, Performance analysis of a windmill with increased power-output due to tipvane induced diffusion of the airstream, Memorandum M-224, Delft University of Technology, Department of Aerospace Engineering.
6. Th. van Holten, Higher-order asymptotic expressions for the velocity field of a propeller duct or an array of tipvanes in axisymmetric flow, Memorandum M-280, Delft University of Technology, Department of Aerospace Engineering.

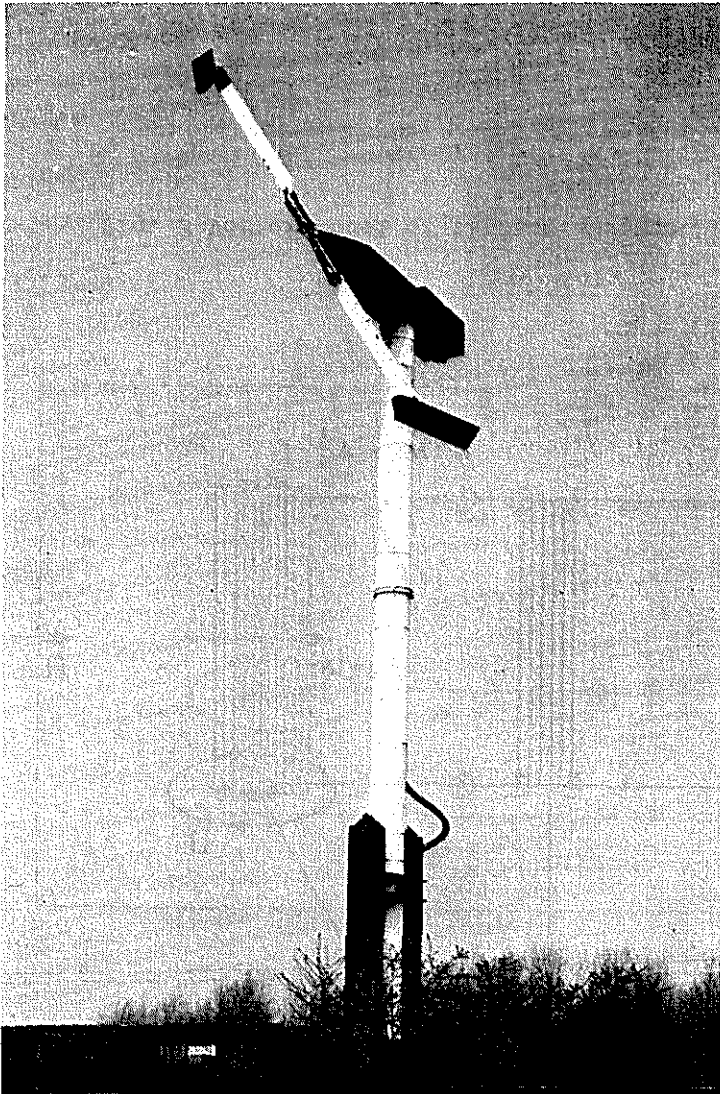


Fig. 1 Full-scale tipvane testrotor,
8.5 meter diameter.

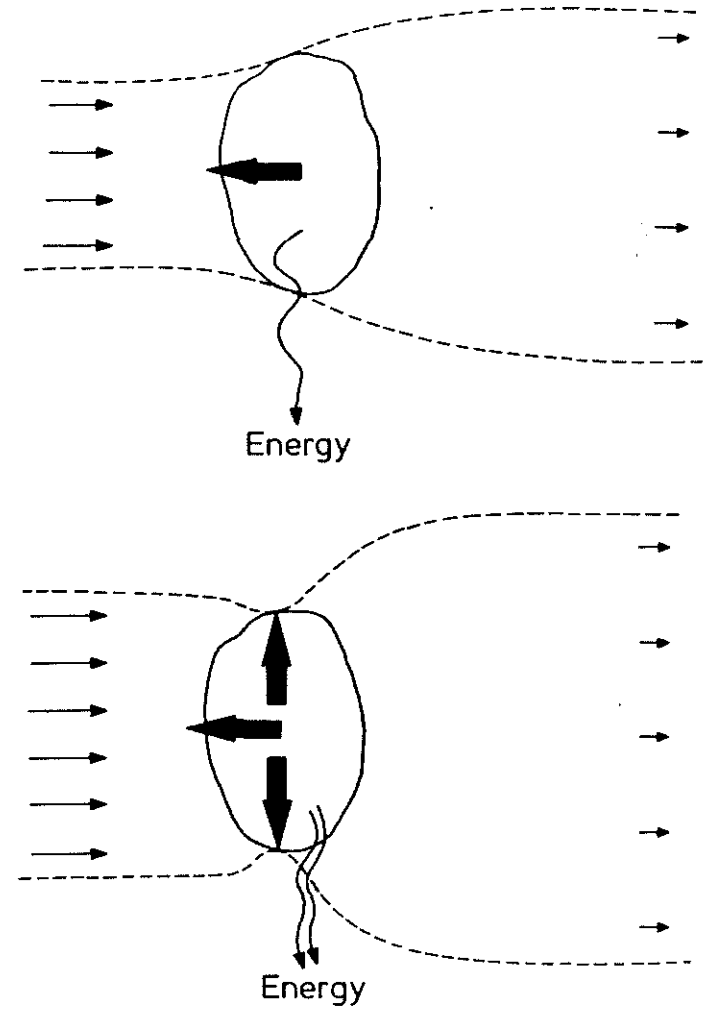


Fig. 2 Flow type for conventional turbine and turbine
with cross-wind forces.

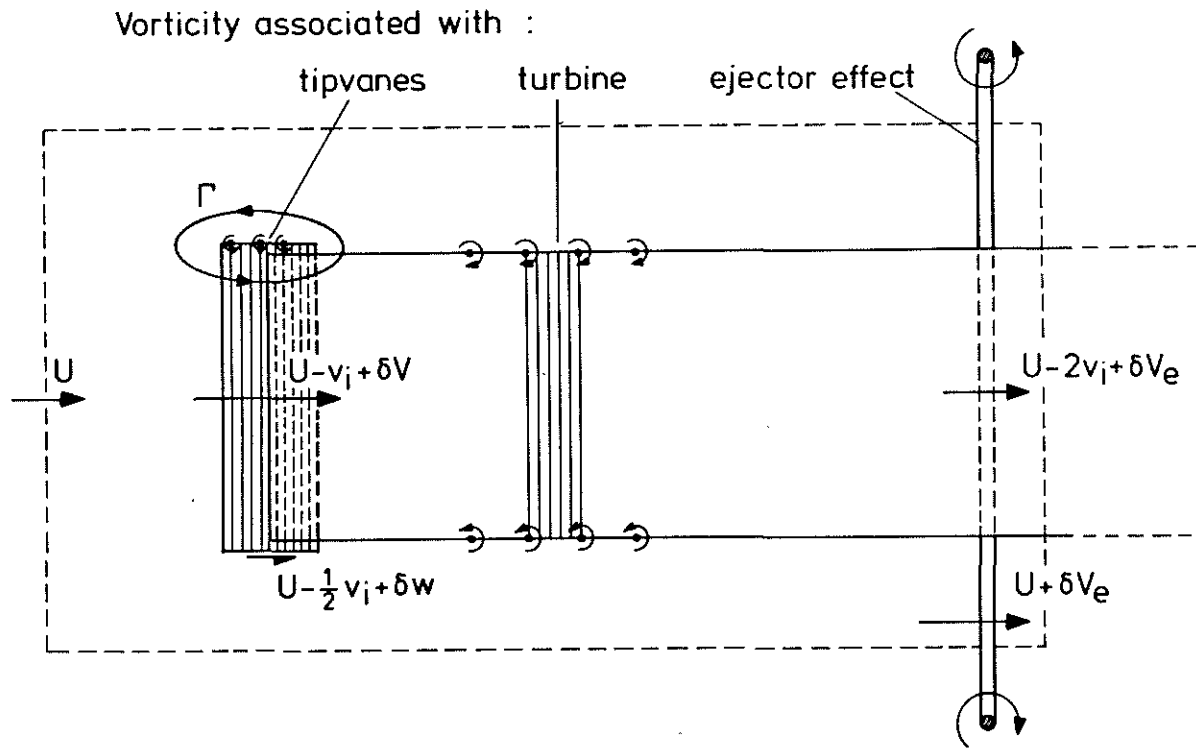


Fig. 3 Vortex model of tipvane-turbine.

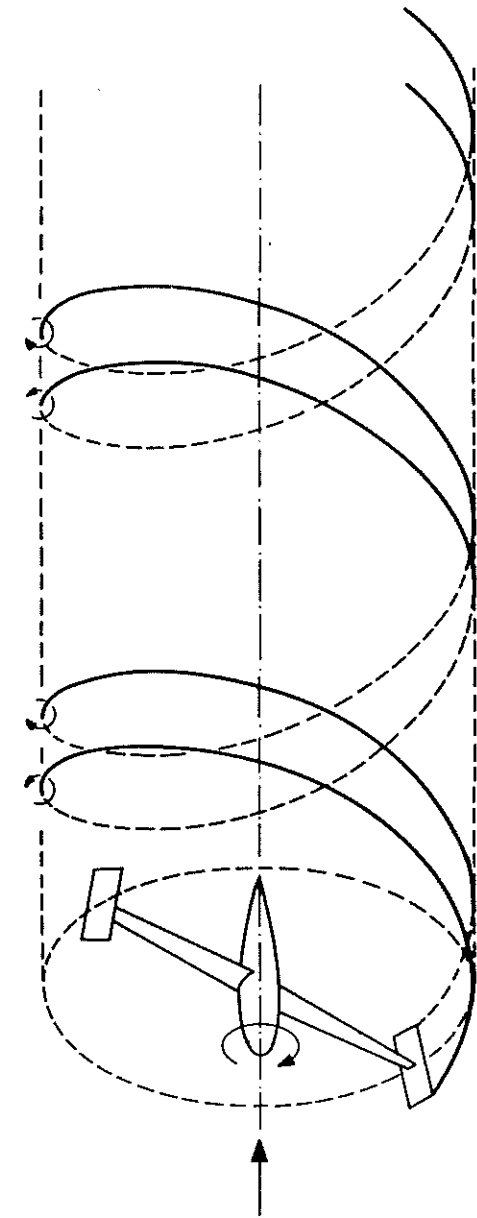


Fig. 4 Undersynchronous operation of tipvane turbine.

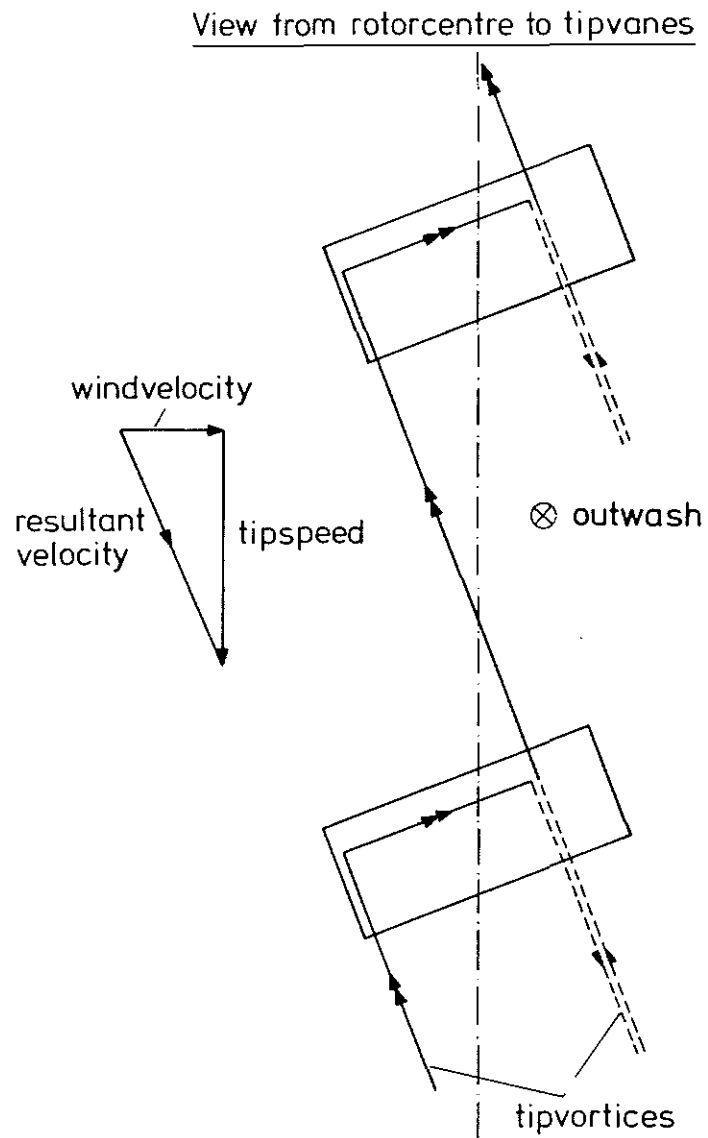


Fig. 5 Oversynchronous operation.

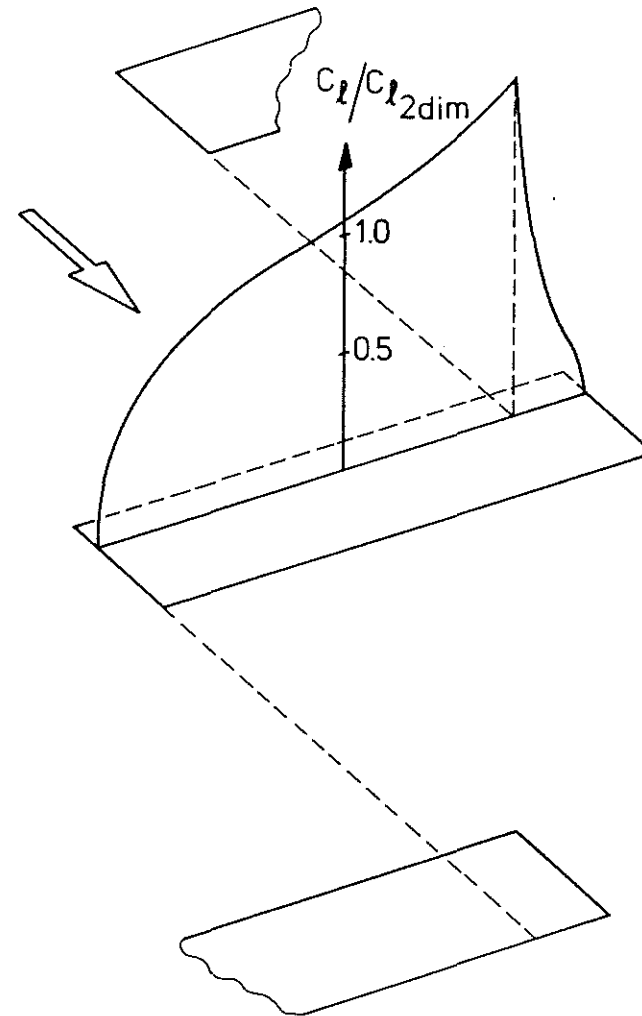


Fig. 6 Liftdistribution on vane during oversynchronous operation.

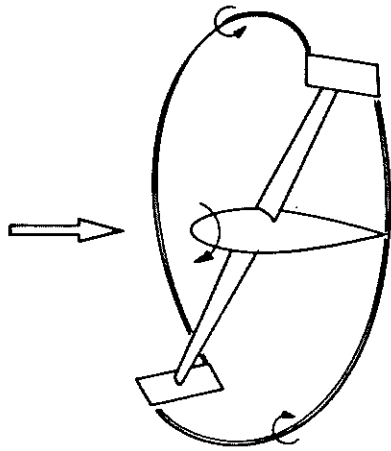


Fig. 7 Saw-tooth vortex during over-synchronous operation

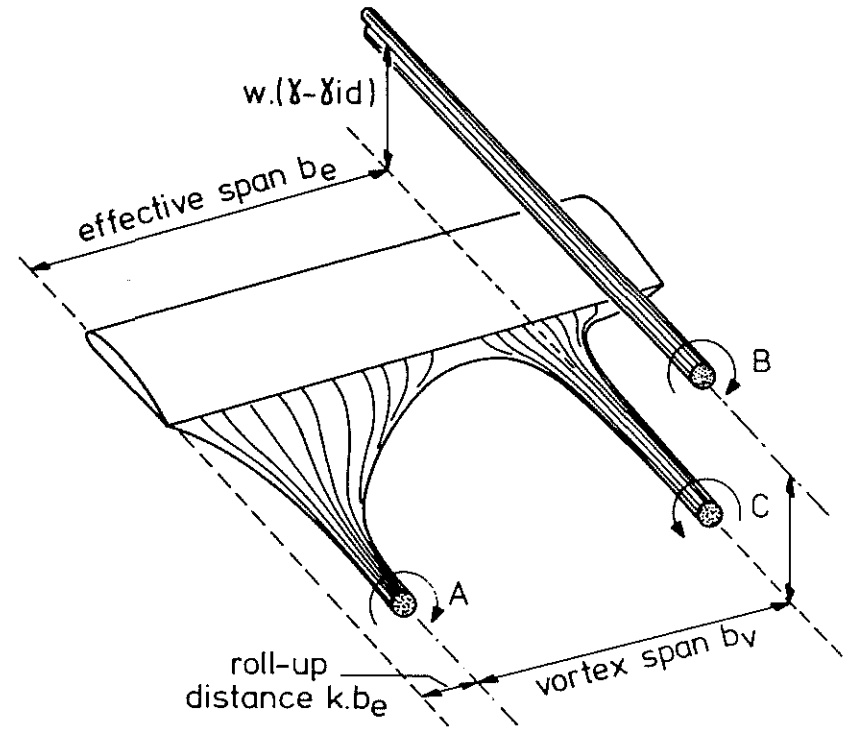
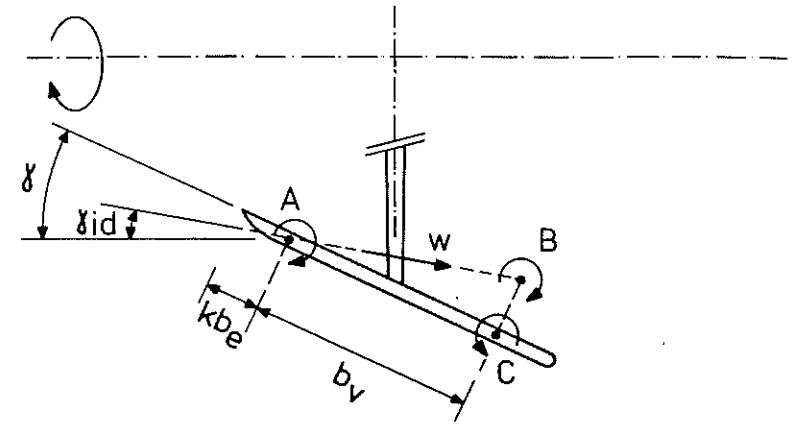


Fig. 8 Off-design condition with vane tilt-angle too large.

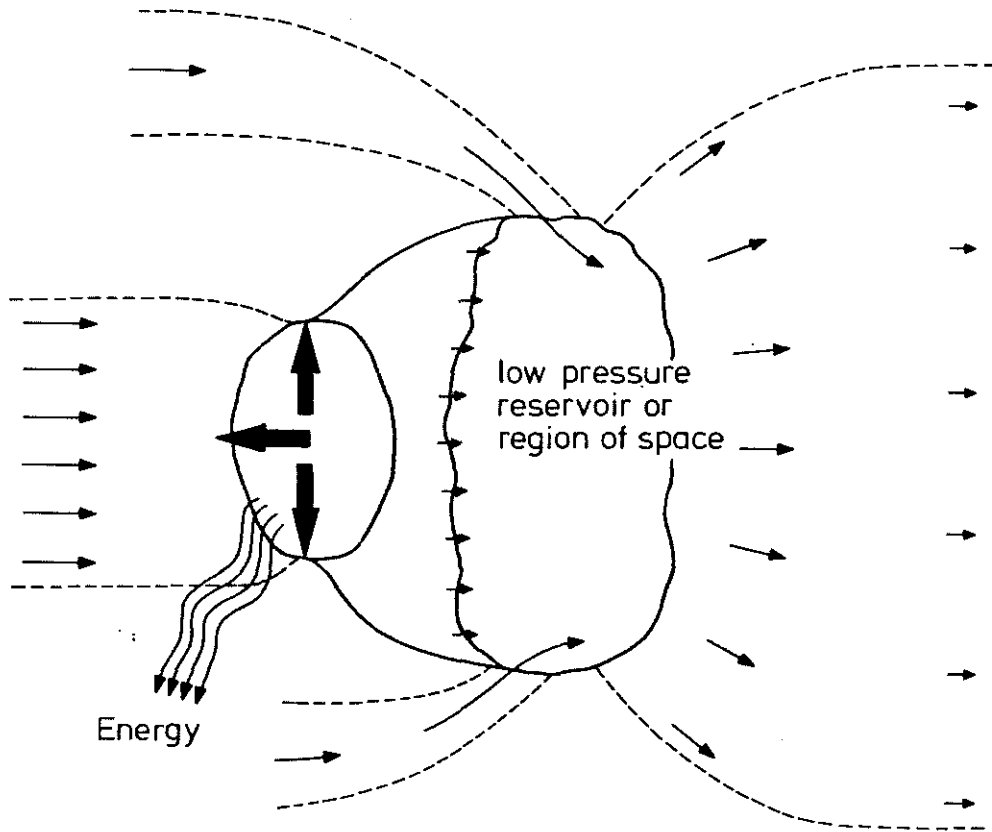


Fig. 9 Physical model explaining ejector-effect

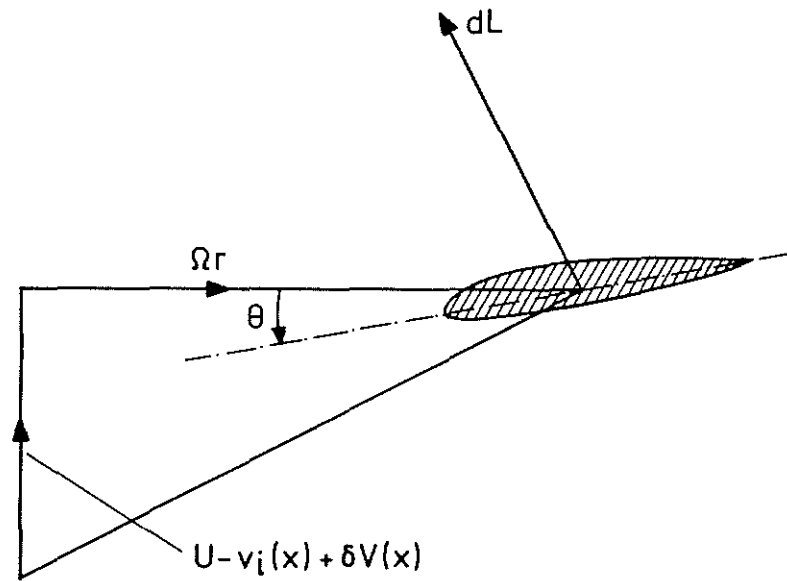


Fig. 10 Velocity diagram for element of powerblade.

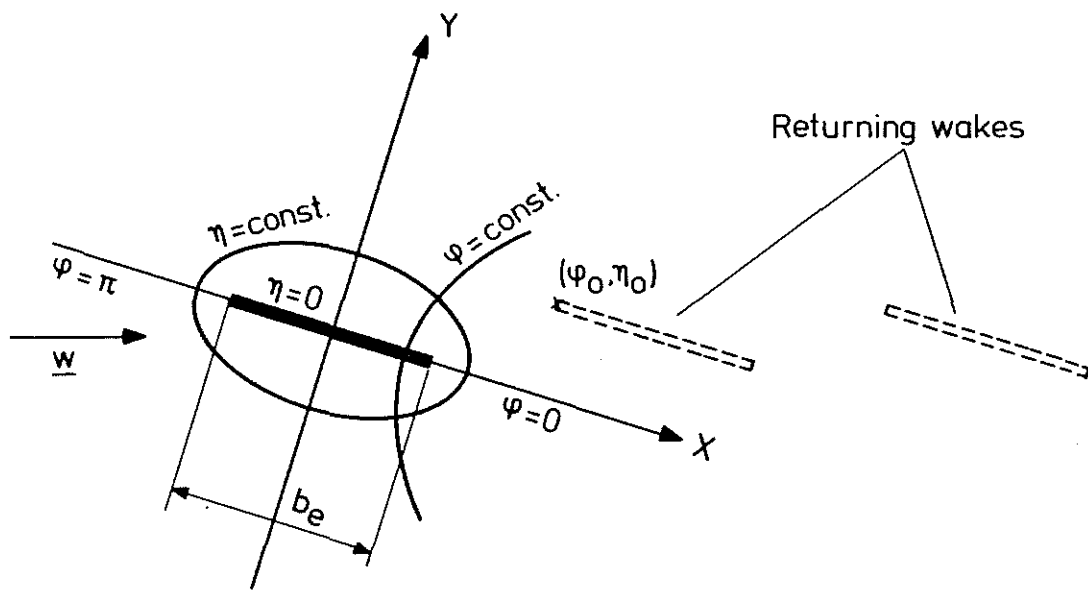


Fig. 11 Analysis of induced velocity in Trefftz-plane.

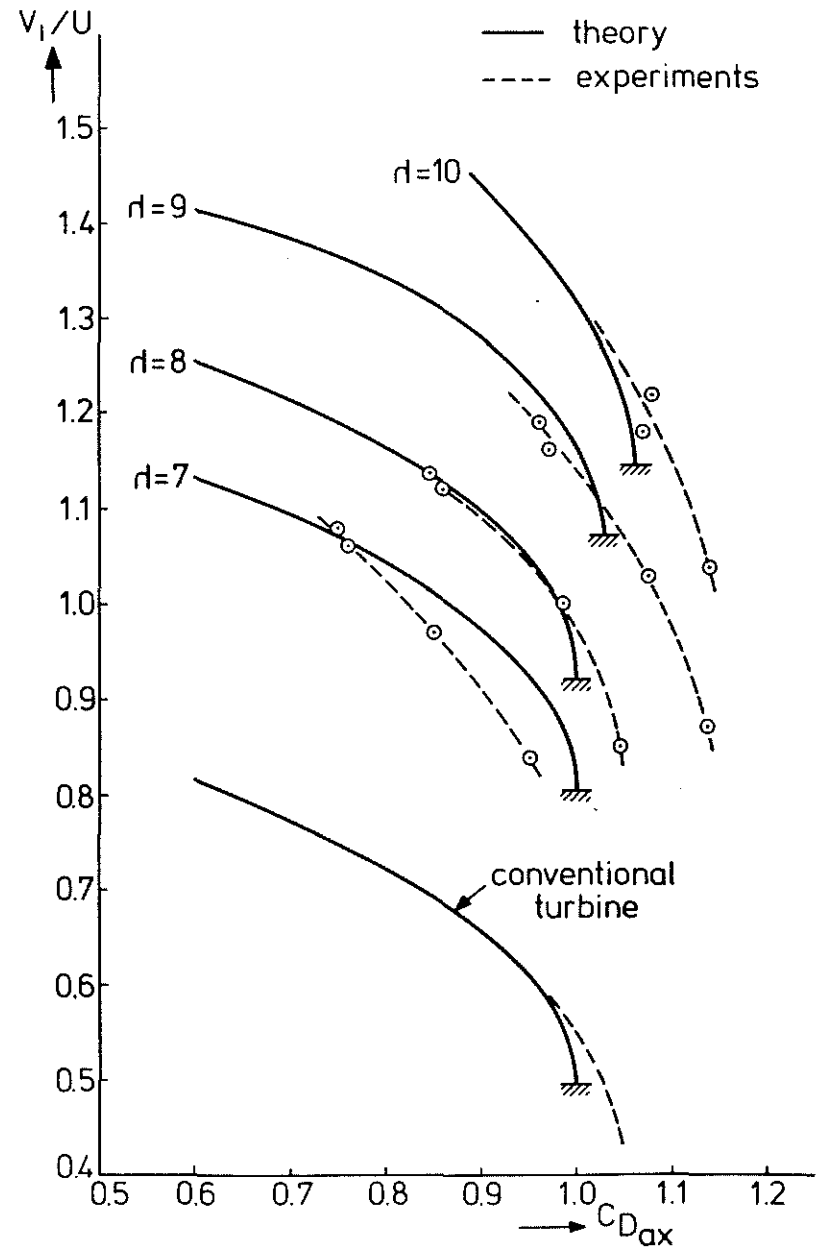


Fig. 12. Calculated and measured diffuser-characteristics of windtunnelmodel with gauze-simulation of p r turbine.

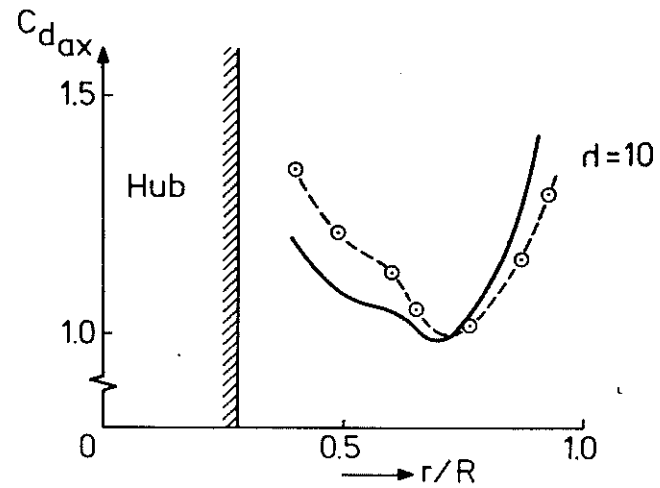
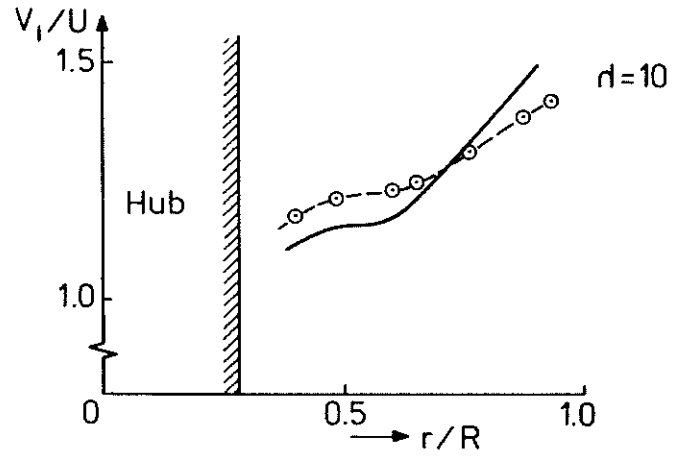


Fig. 13 Calculated and measured distribution of velocity and total pressure-loss in turbine plane

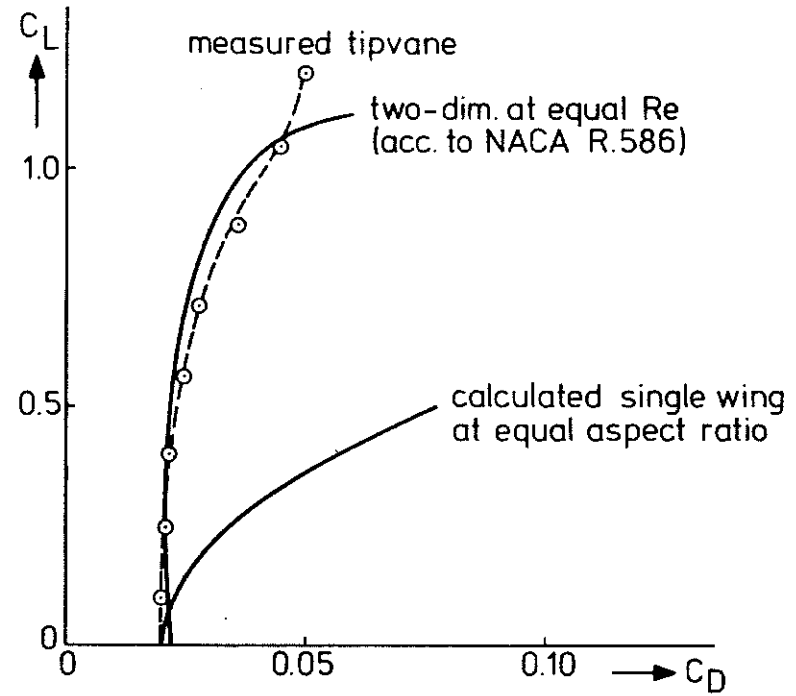


Fig. 14 Measured tipvane dragpolar.

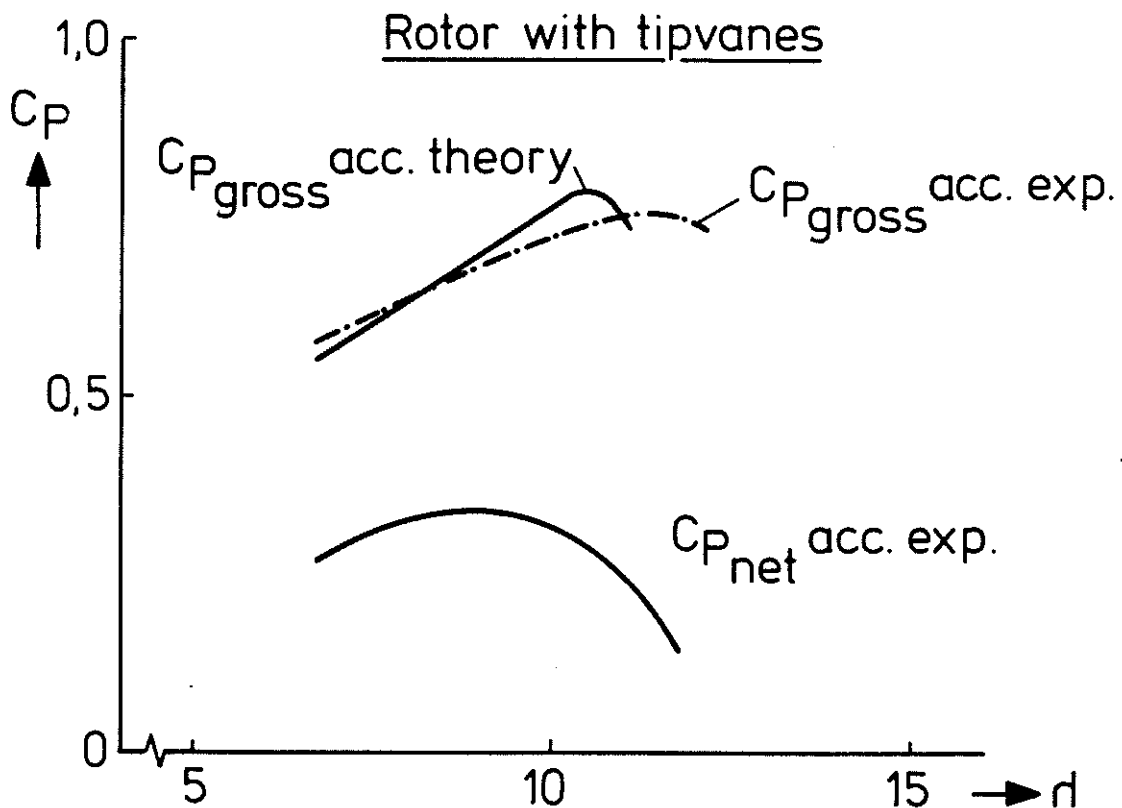
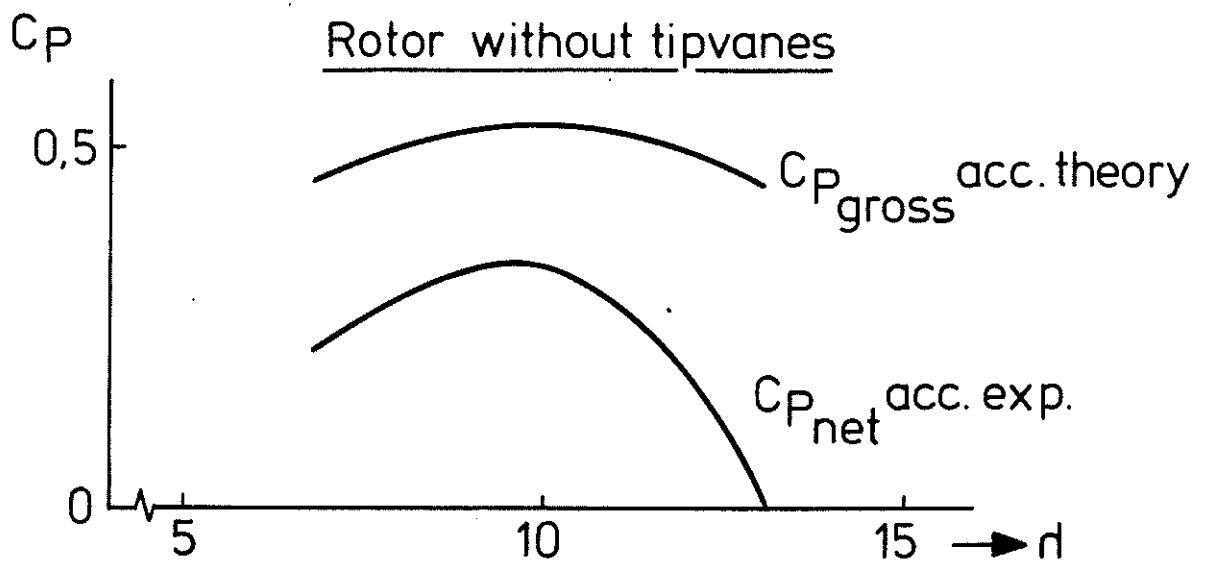


Fig.15: Break-even tests at small vane-lift $C_{L_{vane}} = 0.4$ (vanes just drive themselves). $C_{P_{gross}}$ with tipvanes obtained by adding to experimental $C_{P_{net}}$ the losses as measured on rotor without vanes, as well as adding losses corresponding to separately measured vane-profiledrag.